

# Phase Control of Nonadiabaticity-induced Quantum Chaos in An Optical Lattice

Jiangbin Gong and Paul Brumer

*Chemical Physics Theory Group, University of Toronto, Toronto, Canada M5S 3H6*

(October 31, 2018)

The qualitative nature (i.e. integrable vs. chaotic) of the translational dynamics of a three-level atom in an optical lattice is shown to be controllable by varying the relative laser phase of two standing wave lasers. Control is explained in terms of the nonadiabatic transition between optical potentials and the corresponding regular to chaotic transition in mixed classical-quantum dynamics. The results are of interest to both areas of coherent control and quantum chaos.

PACS numbers: 32.80.Qk, 05.45.Mt, 05.45.Gg

Recent years have witnessed an increasing interest in the coherent control of atomic and molecular processes [1,2]. One central aspect of coherent control is *phase control*, in which different optical phases are introduced into coherent laser-matter interactions in order to manipulate quantum interference effects and thus to achieve target objectives. It has been shown that phase control approaches are widely applicable [1], even to some systems displaying quantum chaotic dynamics [3].

As we show in this letter, optical lattices, of great recent interest [4], provide an important system in which to explore aspects of quantum chaos and coherent control. In particular, we describe the all-optical phase control of the translational motion of atoms in a system that allows chaotic vs. integrable motion depending on the phase shift between two standing-wave laser fields. The control mechanism is shown to originate in the nonadiabatic coupling between different optical potentials as well as in the regular to chaotic transition in a mixed classical-quantum description of the model system. The results are of broad interest to both coherent control and quantum chaos.

Consider a  $\Lambda$ -type 3-level atom moving along two co-propagating standing-wave laser beams, with two lower degenerate levels  $|1\rangle$  and  $|3\rangle$ , and one upper level  $|2\rangle$ . Two laser fields, with different polarizations  $\sigma_+$  and  $\sigma_-$ , couple  $|1\rangle$  with  $|2\rangle$  and  $|2\rangle$  with  $|3\rangle$ , respectively. A closed 3-level  $\Lambda$  configuration of this kind may be realized, for example, in  $^4\text{He}$  using the  $2^3S_1 \rightarrow 2^3P_1$  transition [5]. The laser fields are of the same frequency, with large detuning  $\Delta$  from  $|2\rangle$ . We use  $x, p, M, \Omega_1 (\Omega_2), k_1 (=k_2)$  to represent the position, momentum, atomic mass, the two Rabi frequencies (assumed real) and the two wavevectors, respectively. The relative phase of the two standing-waves is denoted by  $\phi$ . For generality we employ a set of natural units by scaling all the parameters, i.e.,  $x^0 = \lambda$  for  $x$ ,  $p^0 = \hbar/\lambda$  for  $p$ ,  $t^0 = M\lambda^2/\hbar$  for the time variable  $t$ ,  $\Omega^0 = 2/t^0$  for  $\Delta, \Omega_1$  and  $\Omega_2$ . In terms of these units, the dynamical equations do not explicitly contain the atomic mass, the effective wavevector is given by  $k = 2\pi$ , and  $[x, p] = i$  in the full quantum dynamics. In the rotating wave approximation and in the interaction picture, the

Hamiltonian describing the translational motion along the laser beams is  $H = p^2/2 + (V_{ij})$ , with the potential matrix  $(V_{ij})$  ( $i, j = 1, 2, 3$ ) given by

$$(V_{ij}) = \begin{pmatrix} 2\Delta & \Omega_1 \sin(kx) & 0 \\ \Omega_1 \sin(kx) & 0 & \Omega_2 \sin(kx + \phi) \\ 0 & \Omega_2 \sin(kx + \phi) & 2\Delta \end{pmatrix}. \quad (1)$$

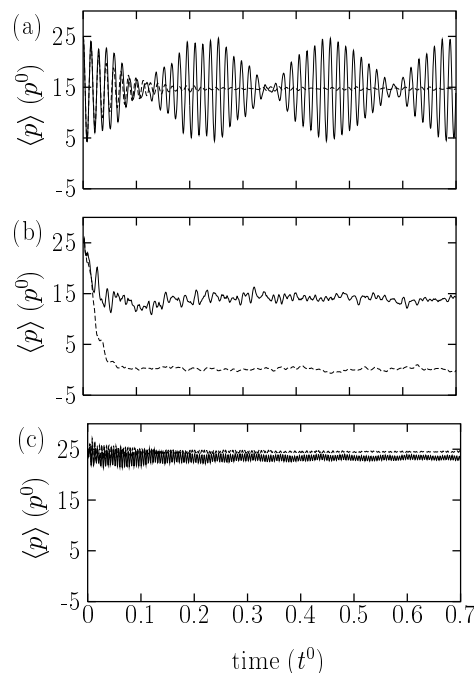


FIG. 1. Time dependence of  $\langle p \rangle$  obtained from quantum wavepacket dynamics calculations (solid lines) and the ensemble statistics in a mixed classical-quantum description (dashed lines). The initial internal state is  $|1\rangle$ , and the  $\langle x \rangle$  and  $\langle p \rangle$  of the initial Gaussian ensemble are 0.0 and 25.0, respectively. The initial variances in position and momentum are chosen to be  $1.0/10\sqrt{2}$  and  $10.0/\sqrt{2}$ , respectively. The relative phase  $\phi$  equals 0.0,  $0.25\pi$ , and  $0.5\pi$  in (a), (b) and (c), respectively.

To demonstrate phase control of the dynamics, consider numerical results for the specific case where (1)

$\Omega_1 = 6.0 \times 10^3$ ,  $\Omega_2 = 7.0 \times 10^3$ ,  $\Delta = 1.5 \times 10^4$ ; (2) the atom is initially in internal state  $|1\rangle$ ; and (3) the average momentum, average position, momentum variance, and position variance of the initial Gaussian wavepacket are given by  $\langle p \rangle = 25.0$ ,  $\langle x \rangle = 0.0$ ,  $\delta p = 10/\sqrt{2}$  and  $\delta x = 1.0/10\sqrt{2}$ , respectively. In  $^4\text{He}$ , this corresponds to  $t^0 \sim 77 \mu\text{sec}$ , the detuning  $\sim 2\pi \cdot 62 \text{ MHz}$  (about 38 times the linewidth of  $|2\rangle$ ), and the initial kinetic temperature  $\sim 29 \mu\text{K}$ . Results for this case represent typical observations for a wide range of system parameters and initial conditions that we have examined [6].

The solid curves in Fig. 1, which contain the essential result of this letter, show the time dependence of the quantum momentum expectation value  $\langle p \rangle$  for time evolving wavepackets for various  $\phi$ . The  $\phi = 0$  case [Fig. 1a] displays a perfectly regular recurrence pattern. By contrast, the  $\phi = 0.25\pi$  case [Fig. 1b] is characteristic of a relaxation process, with significantly irregular oscillations of small amplitude. In addition, the associated power spectrum (not shown) is quite noisy, characteristic of chaos [7]. Further tuning  $\phi$  leads to totally different dynamics: in the  $\phi = 0.5\pi$  case [Fig. 1c],  $\langle p \rangle$  lies very close to its initial value and undergoes regular oscillations, but with a characteristic frequency that is much higher than that in the  $\phi = 0$  case (The dashed curves in Fig. 1 are discussed later below). Clearly, the atom's translational motion undergoes significant qualitative changes with controlled changes in  $\phi$ .

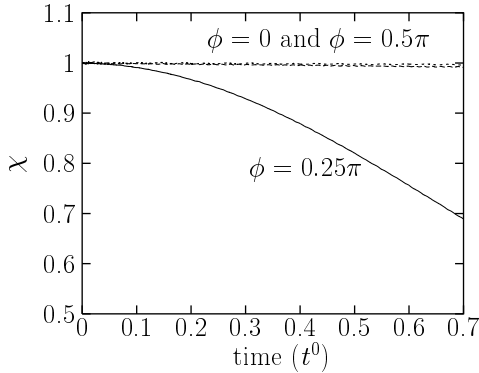


FIG. 2. The sensitivity of the quantum dynamics to slight changes of the relative phase parameter  $\phi$ .  $\chi$  is the absolute value of the overlap between the two time evolving wavefunctions emanating from the same initial state as in Fig. 1, with the relative phase of the two standing-wave laser fields given by  $\phi$  and  $\phi + \pi/400$ .

To demonstrate that this is indeed an integrable to chaotic transition, we consider the sensitivity of the dynamics to slight changes of  $\phi$ . Figure 2 shows the time dependence of the absolute value of the overlap  $\chi$  of two time evolving wavefunctions emanating from the same initial Gaussian wavepacket, with the relative phase of the two laser fields given by  $\phi$  and  $\phi + \pi/400$ , respec-

tively. For  $\phi = 0$  or  $\phi = 0.5\pi$ ,  $\chi$  remains near unity throughout, indicating that the dynamics is insensitive to tiny changes of  $\phi$ . By contrast, for  $\phi = 0.25\pi$ ,  $\chi$  is already less than 0.70 at  $t = 0.7$ . This interesting *hy-persensitivity* [8] to perturbations in the relative phase parameter  $\phi$  further suggests that the  $\phi = 0.25\pi$  case is indicative of quantum chaos.

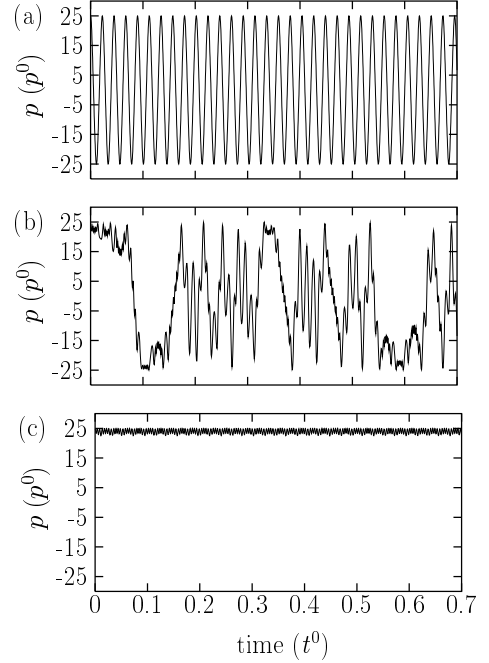


FIG. 3. Time dependence of momentum for classical trajectories obtained by solving Eqs. (2), (3), and (4), with the initial position  $x = 0$  and the initial momentum  $p = 25.0$ . The initial internal state is given by  $|1\rangle$ .  $\phi$  equals 0.0,  $0.25\pi$ , and  $0.5\pi$  in (a), (b) and (c), respectively.

To further substantiate that this is a regular to chaotic transition we consider a mixed classical-quantum description of the dynamics, i.e., where the center-of-mass motion evolves classically on an average potential and where the internal motion is treated quantum mechanically [9,10]. From this perspective, the state of motion is described by a phase space point  $(x, p)$  and an internal wavefunction  $|\psi\rangle = (C_1, C_2, C_3)$ , where  $C_1$ ,  $C_2$ , and  $C_3$  are the projections of the wavefunction onto the three internal levels. The dynamical equations are given by

$$\frac{dx}{dt} = p, \quad (2)$$

$$\begin{aligned} \frac{dp}{dt} &= -\langle \psi | \frac{dV}{dx} | \psi \rangle \\ &= -\Omega_1 k (C_2 C_1^* + C_2^* C_1) \cos(kx) \\ &\quad -\Omega_2 k (C_2 C_3^* + C_2^* C_3) \cos(kx + \phi), \end{aligned} \quad (3)$$

and

$$i \frac{dC_k}{dt} = \sum_{j=1}^3 V_{kj} C_j, \quad k = 1, 2, 3. \quad (4)$$

One can readily solve these equations numerically to obtain  $p(t)$  for the classical translational motion. The results, for the same system parameters and the same initial internal state as in the quantum calculations, but for a single trajectory initially at  $(x, p) = (0.0, 25.0)$ , are shown in Fig. 3. In particular, for  $\phi = 0$  [Fig. 3a] the oscillation of momentum is perfectly regular, in agreement with the regular recurrence pattern in Fig. 1a. By contrast, for  $\phi = 0.25\pi$  [Fig. 3b], the trajectory is highly irregular, with random alternations between fast small-amplitude and slow large-amplitude oscillations. In this case two initially nearby trajectories shows exponential divergence in phase space with an associated Lyapunov exponent of  $\sim 50/t^0$ . This supports the view that the irregular dynamics in Fig. 1b, and the sensitivity of the dynamics to slight changes of  $\phi$  shown in Fig. 2, are indeed due to optical-phase-assisted quantum chaos. Further, in the  $\phi = 0.5\pi$  case [Fig. 3c], the regular classical motion is restored, with a characteristic frequency identical to that in Fig. 1c. Hence optical-phase control is evident in this classical-quantum treatment as well.

An ensemble statistics in the classical treatment of translational motion provides further support. The dashed lines in Fig. 1 display the time dependence of the average momentum  $\langle p \rangle$  for an ensemble of trajectories initially centered at  $x = 0$  and  $p = 25.0$ , with the same initial variances as in the quantum calculations. Each individual trajectory in the ensemble is obtained by solving Eqs. (2) – (4). The quantum-classical correspondence for the regular dynamics at times  $t < 0.15$  in Figs. 1a and 1c is impressive. On the other hand, as seen in Fig. 1b,  $\langle p \rangle$  for the classical ensemble quickly relaxes to zero, whereas  $\langle p \rangle$  for the quantum ensemble remains far away from zero. This quantum-classical difference constitutes an excellent example of quantum suppression of classical chaos in an unbounded Hamiltonian system.

Insight into the origin of phase control can be obtained by considering the dynamics in an adiabatic representation. To do so we introduce an orthogonal transformation  $(O_{ij})$  ( $i, j = 1, 2, 3$ ) to diagonalize the potential matrix  $(V_{ij})$ .  $(O_{ij})$  is given by

$$(O_{ij}) = \begin{pmatrix} \frac{\Omega_1 \sin kx}{\sqrt{2(\eta^2 - \Delta\eta)}} & \frac{\Omega_2 \sin(kx + \phi)}{\xi} & \frac{\Omega_1 \sin(kx)}{\sqrt{2(\eta^2 + \Delta\eta)}} \\ \frac{\eta - \Delta}{\sqrt{2(\eta^2 - \Delta\eta)}} & 0 & \frac{-\eta - \Delta}{\sqrt{2(\eta^2 + \Delta\eta)}} \\ \frac{\Omega_2 \sin(kx + \phi)}{\sqrt{2(\eta^2 - \Delta\eta)}} & \frac{-\Omega_1 \sin(kx)}{\xi} & \frac{\Omega_2 \sin(kx + \phi)}{\sqrt{2(\eta^2 + \Delta\eta)}} \end{pmatrix}, \quad (5)$$

where  $\xi(x, \phi) \equiv \sqrt{\Omega_1^2 \sin^2(kx) + \Omega_2^2 \sin^2(kx + \phi)}$  and

$\eta(x, \phi) \equiv \sqrt{\xi^2(x, \phi) + \Delta^2}$ . Corresponding to the three eigenvectors  $(O_{1j}, O_{2j}, O_{3j})$  ( $j = 1, 2, 3$ ), are three eigenpotentials  $V_i(x, \phi)$  given by  $V_1(x, \phi) = \Delta + \eta(x, \phi)$ , the constant potential  $V_2 = 2\Delta$ , and  $V_3(x, \phi) = \Delta - \eta(x, \phi)$ . For the special case of  $\phi = 0$ ,  $V_1$  and  $V_2$  are degenerate at  $kx = n\pi$ , and the eigenvector  $(O_{12}, O_{22}, O_{32})$  is  $x$ -independent; for the general cases of  $\phi \neq 0$ ,  $V_1(x, \phi) > V_2 > V_3(x, \phi)$ , i.e., the three potential curves do not cross one another. Of particular interest is the constant potential  $V_2$ , associated with the eigenvector  $(O_{12}, O_{22}, O_{32})$ . Since

$$\Omega_1 \sin(kx) O_{12} + \Omega_2 \sin(kx + \phi) O_{32} = 0, \quad (6)$$

$V_2$  results from the complete quantum destructive interference between the two standing-wave laser fields. As such,  $V_2$  is an extension of the “dark optical lattice” in the presence of two counter-propagating plane-wave laser beams [5,11,12].

Consider now transforming Eqs. (3) and (4) to the eigen-potential (adiabatic) representation. Specifically, consider the dynamics in terms of  $\tilde{C}_i$ ,  $i = 1, 2, 3$ , where  $\tilde{C}_i = \sum_{k=1}^3 O_{ki} C_k$ . Using  $\sum_{k=1}^3 O_{ki} O_{kj} = \delta_{ij}$  and  $\sum_{k=1}^3 O_{ki} dO_{kj}/dx = -\sum_{k=1}^3 O_{kj} dO_{ki}/dx$ , Eqs. (3) and (4) can be transformed to

$$\frac{dp}{dt} = -|\tilde{C}_1|^2 \frac{dV_1(x, \phi)}{dx} - |\tilde{C}_3|^2 \frac{dV_3(x, \phi)}{dx}, \quad (7)$$

and

$$i \begin{pmatrix} \frac{d\tilde{C}_1}{dt} \\ \frac{d\tilde{C}_2}{dt} \\ \frac{d\tilde{C}_3}{dt} \end{pmatrix} = \begin{pmatrix} V_1(x, \phi) & it_{12} & -it_{13} \\ -it_{12} & V_2 & -it_{23} \\ it_{13} & it_{23} & V_3(x, \phi) \end{pmatrix} \begin{pmatrix} \tilde{C}_1 \\ \tilde{C}_2 \\ \tilde{C}_3 \end{pmatrix}, \quad (8)$$

where the diagonal terms are the three adiabatic potentials given above, and the potential coupling terms are given by  $t_{12}(x, \phi) = pk\Omega_1\Omega_2 \sin(\phi)/[2\xi^2(\eta^2 - \Delta\eta)]^{1/2}$ ,  $t_{13}(x, \phi) = pk\Delta[\Omega_1^2 \sin(2kx) + \Omega_2^2 \sin(2kx + 2\phi)]/4\eta^2\xi$ , and  $t_{23}(x, \phi) = pk\Omega_1\Omega_2 \sin(\phi)/[2\xi^2(\eta^2 + \Delta\eta)]^{1/2}$  [13]. Note that  $t_{ij}$  ( $i \neq j = 1, 2, 3$ ) is proportional to the momentum  $p$ . Thus, the coupling between optical potentials is due to the nonadiabatic effects associated with translational motion. Further, for the computational example discussed above (and many other cases in which  $\Delta > 0$ ) one has  $\min[V_1(x, \phi) - V_2] \ll \min[V_2 - V_3(x, \phi)]$  and  $t_{12}(x, \phi) \gg t_{23}(x, \phi)$ , suggesting that  $V_3(x, \phi)$  is effectively decoupled from  $V_1(x, \phi)$  and  $V_2$ . Note also that at the initial location  $x = 0$ , the initial internal state  $|1\rangle$  is a superposition state of the two eigenvectors associated with  $V_1$  and  $V_2$  for  $\phi = 0$ , and reduces to the eigenvector associated with  $V_2$  for  $\phi \neq 0$ .

The key role of the relative laser phase  $\phi$  becomes clear as one compares the magnitude of the nonadiabatic coupling term  $t_{12}(x, \phi)$  with that of  $(V_1 - V_2)$ . For case (a),  $\phi = 0$  and  $t_{12}(x, \phi = 0) = 0$ , so the dynamics is adiabatic. Thus, in the case of Fig. 1a, the quantum ensemble divides into two sub-ensembles: one is

trapped in one well of  $V_1$  around  $x = 0$  and undergoes periodic oscillations, and the other experiences the trivial motion on the constant potential  $V_2$ . For case (b),  $\phi = 0.25\pi$ . Here the smallest gap between  $V_1$  and  $V_2$  is given by  $g(\phi) = \sqrt{A^2(\phi) + \Delta^2} - \Delta$ , where  $A^2(\phi) = [\Omega_1^2 + \Omega_2^2 - \sqrt{\Omega_1^4 + \Omega_2^4 + 2\Omega_1^2\Omega_2^2 \cos(2\phi)}]/2$ . The corresponding ratio of the potential coupling term  $t_{12}$  to  $g(\phi)$  is given by

$$T(\phi) = \frac{pk\Omega_1\Omega_2 \sin(\phi)}{\sqrt{2}[A^2(\phi) + \Delta^2]^{1/4}A(\phi)g^{3/2}(\phi)}. \quad (9)$$

Since  $T(\phi = 0.25\pi) \approx 1.0$ , the magnitude of the nonadiabatic coupling is comparable to that of  $(V_1 - V_2)$ , resulting in strong nonadiabatic effects. Thus, the chaotic motion seen in Fig. 3b is induced by the significant nonadiabatic coupling between the two simple one-dimensional potentials  $V_1$  and  $V_2$ . Finally, for case (c),  $\phi = 0.5\pi$ . Here  $T(\phi = 0.5\pi) = \min[T(\phi)] \approx 0.16$ , i.e., the nonadiabatic coupling is appreciably weaker than in the case of  $\phi = 0.25\pi$ . As such, the translational motion, initially launched on the adiabatic potential  $V_2$ , would essentially remain on  $V_2$ , with small perturbations from the insignificant Rabi population oscillation between  $V_1$  and  $V_2$ . To further confirm this picture, one finds that the characteristic frequency of the regular dynamics in Fig. 1c and Fig. 3c is  $\sim 1425$ , a value consistent with the Rabi frequencies given by  $\sqrt{(V_1 - V_2)^2 + 4t_{12}^2}$  [see Eq. (8)].

A number of additional remarks are in order. First, the two-standing-wave configuration is essential in this system. That is, if either or both of the two standing-wave fields are replaced by a traveling-wave, the nonadiabatic coupling or the spacing between  $V_1$  and  $V_2$  is no longer a sensitive function of  $\phi$ , and there is no significant phase control. On the other hand, a three-level atom in two standing-wave laser fields of different but commensurate frequencies also shows dynamics which is controllable by changing  $\phi$  [14]. Second, in contrast to some recent studies on optical-magneto lattice [15,16], the coupling between different optical potentials discussed above is not due to additional magnetic fields, but directly due to nonadiabaticity. Further, unlike the work in Ref. [16], here we have observed clear signatures of quantum chaos in the quantum dynamics. Thus, this model is the first all-optics realization of nonadiabaticity-induced quantum chaos, a phenomenon first discovered in molecular systems [17]. Third, in this work we have neglected decoherence effects (e.g., due to the spontaneous emission from the excited state  $|2\rangle$ ). It would be interesting to explore how decoherence affects phase control and quantum-classical correspondence in this system.

In conclusion, we have demonstrated optical phase control of nonadiabaticity-induced quantum chaos in a  $\Lambda$ -type 3-level system in a two-standing-wave optical lattice. The results shown in Fig. 1 are but samples of the observable, controllable, behavior. Further, the func-

tional dependence on  $\phi$  has been exposed analytically, which can serve to guide experimental studies of the  $\phi$ -dependent regular to chaotic transition. Recent experimental progress in atom optics and quantum chaos [4,5,12,15,18] suggests that the results should be experimentally achievable with existent technology. This work was supported by the U.S. Office of Naval Research and the Natural Sciences and Engineering Research Council of Canada. J.G. is a Henry Croft Postdoctoral Fellow in Theoretical Chemical Physics.

- 
- [1] M. Shapiro and P. Brumer, *Adv. Atom., Mol. and Opt. Phys.*, **42**, 287 (2000).
  - [2] S.A. Rice and M. Zhao, *Optical Control of Molecular Dynamics* (John Wiley, New York, 2000).
  - [3] J. Gong and P. Brumer, *Phys. Rev. Lett.* **86**, 1741 (2001); *J. Chem. Phys.* **115**, 3590 (2001); D. Abrashkevich, M. Shapiro and P. Brumer, *J. Chem. Phys.* (in press).
  - [4] F.L. Moore *et al.*, *Phys. Rev. Lett.* **75**, 4598 (1995); B.G. Klappauf *et al.*, *Phys. Rev. Lett.* **81**, 1203 (1998); H. Ammann *et al.*, *Phys. Rev. Lett.* **80**, 4111 (1998); J. Ringot, *et al.*, *Phys. Rev. Lett.* **85**, 2741 (2000); M.B. d'Arcy *et al.*, *Phys. Rev. Lett.* **87**, 074102 (2001).
  - [5] A. Aspect *et al.*, *Phys. Rev. Lett.* **61**, 826 (1988).
  - [6] The system parameters and the initial conditions should be chosen to ensure that the population on level  $|2\rangle$  is small ( $< 2\%$  in the present case) so that spontaneous emission effects will be insignificant. It is also desirable to ensure negligible tunneling effects between different wells of  $V_1$  so as to achieve good quantum-classical correspondence.
  - [7] R.S. Dumont and P. Brumer, *J. Chem. Phys.* **88**, 1481 (1988).
  - [8] R. Schack and C.M. Caves, *Phys. Rev. Lett.* **71**, 525 (1993); A. Peres, *Phys. Rev. A* **30**, 1610 (1984).
  - [9] J.C. Tully and R.K. Preston, *J. Chem. Phys.* **55**, 562 (1971).
  - [10] R. Blümel and B. Esser, *Phys. Rev. Lett.* **72**, 3658 (1994).
  - [11] R. Dum and M. Olshanii, *Phys. Rev. Lett.* **76**, 1788 (1996).
  - [12] S.K. Dutta, B.K. Teo, and G. Raithel, *Phys. Rev. Lett.* **83**, 1934 (1999).
  - [13] The mixed classical-quantum treatment automatically neglects the optical Gauge potential [11,12], which is not of much interest as far as the nonadiabatic coupling is concerned.
  - [14] J. Gong and P. Brumer, manuscript in preparation.
  - [15] D.L. Haycock *et al.*, *Phys. Rev. Lett.* **85**, 3365 (2000).
  - [16] S. Ghose, P.M. Alsing, and I.H. Deutsch, preprint quant-ph/0102085.
  - [17] E.J. Heller, *J. Chem. Phys.* **92**, 1718 (1990); H. Schanz and B. Esser, *Phys. Rev. A* **55**, 3375 (1997); H. Fujisaki and K. Takatsuka, *Phys. Rev. E* **63**, 066221 (2001).
  - [18] D.A. Steck, W.H. Oskay, and M.G. Raizen, *Science* **293**, 274 (2001); W.K. Hensinger *et al.*, *Nature* **412**, 52 (2001).